Advances in Water Resources 75 (2015) 105–117

Contents lists available at ScienceDirect

Advances in Water Resources

journal homepage: www.elsevier.com/locate/advwatres

Urban flood modelling combining top-view LiDAR data with ground-view SfM observations

Vorawit Meesuk [a,b,*], Zoran Vojinovic [a,1], Arthur E. Mynett [a,c,2], Ahmad F. Abdullah [d,3]

[a] UNESCO-IHE Institute for Water Education, Westvest 7, 2611 AX Delft, The Netherlands
[b] Hydro and Agro Informatics Institute, eighth floor, Bangkok Thai Tower 108, Rangnam Rd, Phayathai, Ratchatewi, Bangkok 10400, Thailand
[c] Delft University of Technology, Faculty of Civil Engineering and Geosciences, Stevinweg 1, 2628 CN Delft, The Netherlands
[d] Universiti Putra Malaysia, 43400 UPM-Serdang, Malaysia

ARTICLE INFO

Article history:
Received 23 April 2014
Received in revised form 10 September 2014
Accepted 17 November 2014
Available online 25 November 2014

Keywords:
Light Detection and Ranging (LiDAR)
High-resolution topographic information
Structure from Motion (SfM)
Multidimensional Fusion of Views (MFV)
Digital Terrain Model (DTM)
Urban flood modelling (UFM)

ABSTRACT

Remote Sensing technologies are capable of providing high-resolution spatial data needed to set up advanced flood simulation models. Amongst them, aerial Light Detection and Ranging (LiDAR) surveys or Airborne Laser Scanner (ALS) systems have long been used to provide digital topographic maps. Nowadays, Remote Sensing data are commonly used to create Digital Terrain Models (DTMs) for detailed urban-flood modelling. However, the difficulty of relying on top-view LiDAR data only is that it cannot detect whether passages for floodwaters are hidden underneath vegetated areas or beneath overarching structures such as roads, railroads, and bridges. Such (hidden) small urban features can play an important role in urban flood propagation. In this paper, a complex urban area of Kuala Lumpur, Malaysia was chosen as a study area to simulate the extreme flooding event that occurred in 2003. Three different DTMs were generated and used as input for a two-dimensional (2D) urban flood model. A top-view LiDAR approach was used to create two DTMs: (i) a standard LiDAR-DTM and (ii) a Filtered LiDAR-DTM taking into account specific ground-view features. In addition, a Structure from Motion (SfM) approach was used to detect hidden urban features from a sequence of ground-view images; these ground-view SfM data were then combined with top-view Filtered LiDAR data to create (iii) a novel Multidimensional Fusion of Views-Digital Terrain Model (MFV-DTM). These DTMs were then used as a basis for the 2D urban flood model. The resulting dynamic flood maps are compared with observations at six measurement locations. It was found that when applying only top-view DTMs as input data, the flood simulation results appear to have mismatches in both floodwater depths and flood propagation patterns. In contrast, when employing the top-ground-view fusion approach (MFV-DTM), the results not only show a good agreement in floodwater depth, but also simulate more correctly the floodwater dynamics around small urban feature. Overall, the new multi-view approach of combining top-view LiDAR data with ground-view SfM observations shows a good potential for creating an accurate digital terrain map which can be then used as an input for a numerical urban flood model.

1. Introduction

Flooding can either come directly from excessive rainfall in urban areas (i.e., pluvial floods), from overbank flows of rivers (i.e., fluvial floods), spillage from lakes and reservoirs, from coastal surges, and high tides (i.e., coastal floods) or from their combination thereof. Damages and losses cannot be completely avoided when major floods occur, but flood preparedness can help to considerably reduce both flood damages and number of lives lost [27,37,41]. Urban flood modelling provides an important tool to simulate flood dynamics prior to occurrence, anticipating the rate of water level rise, estimating the evolution of the flood extent, indicating the expected areas of high flood hazard, and identifying the lead time including escape routes for emergency management [39].

One dimensional (1D) numerical models are commonly used as standard hydraulic simulation tools to forecast floodwater flows and floodwater depths in open channels and pipe networks.

* Corresponding author at: UNESCO-IHE Institute for Water Education, WSE, PO Box 3015, 2601 DA Delft, The Netherlands. Tel.: +31 1 5215 1821.
E-mail addresses: v.meesuk@unesco-ihe.org (V. Meesuk), z.vojinovic@unesco-ihe.org (Z. Vojinovic), a.mynett@unesco-ihe.org (A.E. Mynett), fikri@eng.upm.edu.my (A.F. Abdullah).
[1] Tel.: +31 1 5215 1804.
[2] Tel.: +31 1 5215 1747.
[3] Tel.: +60 3 8946 4337.

http://dx.doi.org/10.1016/j.advwatres.2014.11.008
0309-1708/

However, when extreme floods occur, discharges and water levels may exceed their bank-full discharge values and overflow. A 1D approach will then no longer be adequate to model the flows of excess floodwaters spilling into the urban floodplains [12,28]. In that case, a fully two dimensional (2D) numerical model is needed to simulate the floodwater dynamics in urban areas [7,16,31,35,42]. Alternatively, if the river flow pertains during the urban inundation, a 2D approach with or without a coupled 1D–2D approach can be an adequate to estimate the propagation of excess floodwaters, spilled from the 1D river system onto the 2D terrain [6,22,28]. Obtaining the topographic data in rural, peri-urban, or urban areas is crucial for an effective flood mapping. Such data may contain highly irregular geometries from terrains, vegetation, and man-made structures. This is particularly true for complex urban areas where proper capturing of such geometries is often difficult and it requires processing of high-resolution topographic data [50].

Emerging Remote Sensing technologies are nowadays capable of providing high-resolution topographic data in 2D or even in 3D space and can be used to set up more advanced urban flood models. Amongst them, Light Detection and Ranging (LiDAR) systems have long received considerable attention due to their precise measurement capabilities. LiDAR can provide high-resolution data, which are capable of creating Digital Surface Models (DSMs) and Digital Terrain Models (DTMs) for flood modelling purposes [5,40,52]. LiDAR systems can be mounted on an aircraft (so-called Airborne Laser Scanners – ALS) or used on the ground (referred to as Terrestrial Laser Scanners – TLS). Despite their powerful capabilities, aerial LiDAR has a difficulty to detect floodwater passages under large trees or under urban structures such as sky-train tracks or crosscutting alleyways.

This is where employing the Structure from Motion (SfM) technique can provide benefits to enhance aerial LiDAR data. Through advanced photogrammetry and computer vision techniques, SfM makes it possible to construct 3D information from the different viewpoints of overlapping 2D photos [15]. Such overlapping photos can be easily taken by using consumer digital cameras or video camcorders.

In this paper, an extreme flooding event of June 10th, 2003 in downtown Kuala Lumpur, Malaysia was chosen to serve as a case study for exploring the benefits of the new technique. First, high-resolution topographic data from top-view LiDAR systems were obtained and processed, and then results from ground-view SfM techniques were added. In total, three different DTMs were created: two from using a top-view approach, viz. (i) a standard LiDAR-DTM and (ii) a Filtered LiDAR-DTM, and a third one using (iii) a blended multi-view approach by a novel Multidimensional Fusion of Views-Digital Terrain Model (MFV-DTM). All three DTMs were used as input for a coupled 1D–2D flood model, and their results were evaluated at six measurement locations.

2. Urban flood modelling computational framework

Where flood flows are confined to well-defined conduits, a 1D model can usually be instantiated reliably, and therefore be used to generate results safe for decision-making. For a long time already, one dimensional (1D) numerical models have been used to simulate water flows in open channels, rivers, and pipe networks where the longitudinal length scale vastly exceeds the lateral dimensions. In 1D river modelling, a series of cross-sections spaced at regular intervals are used to set up the model schematization (see Fig. 1). Echo sounder surveys or other types of field equipment are commonly employed to determine the river bathymetries and cross-sectional profiles. For 1D open channel flow, the governing equations describing the changes in flow velocity and water depth

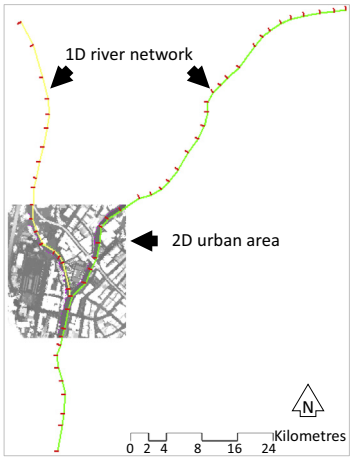

Fig. 1. Example of the coupled 1D–2D modelling approach: the two river branches are represented by a 1D model, and the urban area (street map inside the box) is shown by a 2D schematization.

are based on the conservation principles of mass and momentum and are referred to as the De Saint Venant equations [10]. Although 1D models are capable of capturing the main flow characteristics in two confluent river branches (see Fig. 1), they are not entirely suitable to represent 2D flows along peri-urban and urban areas [18–20]. However, urban floods are normally highly complex in terms of their flows, in the sense that the morphology of the urban surface is eminently artificial, with its highly irregular geometry, which is often contrary to natural flow paths. Modelling flows in such complex geometrical situations is difficult. Small geometric 'discontinuities' such as road or pavement curbs can play a significant role in diverting the shallow flows that are generated in urban environments. Head losses due to flow over or round such structures are difficult to accommodate. Frequently the urban flows are super-critical whereas many of the available modelling products, although they simulate flows that are in reality super-critical, in practice they use modified sub-critical flow algorithms. There is also the issue of treating the transition from channel flows to over-ground shallow depth flows. This necessitates coupling the simulations of 1D and 2D modelling systems [48], both the river network and the urban area can be taken into account [45].

In order to adequately represent urban topography in a numerical model, including drainage network layout, Remote Sensing technologies have proved invaluable for this purpose. Top-view Remote Sensing techniques are able to identify the dominant urban flow pathways based on the urban topography. However, some features may be obscured (e.g., underpasses of elevated roads, sky-train tracks, high trees), and other small urban features (e.g., archways, pavement kerbs, small alleys) may not be easily detected. Nevertheless, such small urban features can play a significant role in diverting shallow flows along roads, through fences, and around buildings. Simulating floodwater flows in such complex geometrical situations is difficult and should be based on the full 2D numerical equations. Clearly, a coupled 1D–2D modelling approach requires longer computational time and greater calibration efforts than a simple 1D schematization. The high-resolution topographic data required to construct the Digital Terrain Model (DTM), the appropriate resistance coefficients, and initial and boundary conditions (discharges, water levels), are all vital information needed to run the coupled 1D–2D model (see the flowchart description in Fig. 2).

3. Topographic data collection for urban flood modelling

A Digital Surface Model (DSM) as obtained from Remote Sensing images contains the elevation of all surfaces, including

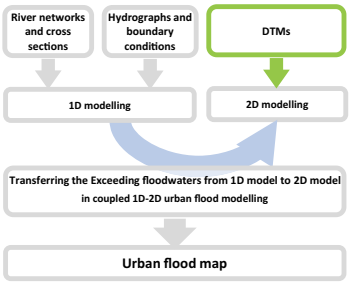

Fig. 2. Coupled 1D–2D model architecture.

buildings, elevated roads, and high trees, as well as the ground surface in the open space in order to construct a Digital Terrain Model (DTM) that accurately represents the terrain surface including underpasses and so-called 'hidden features'. These topographic data can be collected in different ways (e.g., from Stereo Photography, Light Detection and Ranging – LiDAR, Structure-from Motion – SfM) and from different viewpoints (i.e., top-view, ground-view, multi-views) as discussed hereafter.

3.1. Data from top-view LiDAR

Aerial Light Detection and Ranging (LiDAR) surveys have been widely used to create high-resolution topographic elevation data. When obtaining the data from top views, the LiDAR emits light and measures scattered light properties from the ground objects, providing an accurate topographic data with extremely large number of elevation points – called point-cloud data. In LiDAR system, the time-of-flight and phase-shift laser scanner systems are commonly used to establish range measurements. The phase-shift system is more accurate, but its range is shorter than the time-of-flight system [32]. A modified or special airborne platform is needed to carry out all these heavy equipments; LiDAR systems, global positioning systems (GPS), and inertial measurement units (IMU). The platform normally flies to maintain side laps of each flying path between 40% and 60%. The GPS system calculates the relative global positions at sub-metre accuracy, whereas the IMU system records directions and movements to substitute miscalculations of positions when GPS signals are weak.

Applying top-view point-cloud data for flood modelling can significantly improve the accuracy of flood simulation results [21,29,50,51]. Razafison et al. [33] noted that in particular hidden and covered structures could have a major impact on flood propagation and flow dynamics. Mitasova et al. [30] investigated the effect of changing surface elevations; others [49,51] explored the effect of different surface resolutions in their simulations.

3.2. Data from Filtered top-view LiDAR

The steps in LiDAR data processing include 'modelling of systematic errors', 'filtering', 'feature detection', and 'thinning'. Of these steps, filtering and quality control pose the greatest challenges, consuming an estimated 60–80% of the processing time, thus underlining the necessity for on-going research in this area [48]. For more accurate representation of the actual surface, the process of removing points from a mixture of top-view and ground-view measurements is referred to as filtering and classification. To date, a number of filtering and classification algorithms have been developed. Some of these algorithms have been published while others are not known in detail because of proprietary restrictions. The following sections describe some of the existing filter algorithms and improvement of one of these algorithms, so it can be more suitable for urban flood modelling work.

Applying filtering algorithms to top-view LiDAR data can avoid situations where some high obstacles (e.g., elevated roads, sky-train tracks, high trees) may give rise to obstructing floodwater flows. Hence, creating better DTMs can create a more realistic flood simulation results [1,2]. Applying filtering methods can remove some obstructing features, but cannot reconstruct small urban features (e.g., alleyways, under-passages, kerbs) hidden beneath vegetation and structures. These hidden urban features can have considerable effects on floodwater dynamics and predictions in 2D flood simulation results [4,17,23].

3.3. Data from ground-view Structure from Motion

By merging computer vision techniques with advanced photogrammetry, high-resolution topographic maps can be created. The so-called Structure from Motion (SfM) technique is capable of creating very high-resolution topographic data. At almost the same data obtained by aerial LiDAR system, the SfM data have accuracy within ±0.5 m or even better – typically depending on the distance of the camera positions to the objects and the photo resolutions [54]. Unlike traditional photogrammetry techniques, using the SfM technique has a large number of improvements. Rather using the complex metric cameras, the low cost of digital cameras can be adequate to the SfM technique. The digital cameras have been dramatically improved, a number of lens calibration methods have also been developed for a long time already [9,34]. Capturing the scenes using such digital cameras also has some benefits: easy accessibility, user-friendly experiences, and fit for purpose in terms of the data resolutions and coverage areas [54]. It is also easy to mount the cameras on cars, mopeds, or even hand-held devices can be used. Correspondingly, the SfM data can be obtained from different viewpoints, e.g., top-view SfM [53] or ground-view SfM [44,47]. Although a low-cost digital camera can capture the high-resolution photos – fast and easy, a computational efficiency is generally at odds with the fine-resolution demands of data processing. The parallel processing can help to minimise the computational time by increasing the number of Central Processing Unit (CPU) and/or the Graphics Processing Unit (GPU) cores [24,55,56]. However, it is not clear whether the similar improvement in performance can be significantly achieved for the entire city, and how many parallel computing cores are optimal and cost effective.

The process of creating the ground-view SfM data starts with capturing the overlapping 2D photo scenes and proceeds by using a digital camera or a digital video camcorder. If the videos are recorded, the video files should be separated into a series of continuous photos. Then, some features are identified in each pair of overlapping photos by using feature detection methods (e.g., SiftGPU [55] modified from the original SIFT [26] with an advanced Graphics Processing Unit (GPU) implementation). After that, the detected features are is used to calculate extrinsic parameters, which can be used to recover camera positions from correlative rotations, projections, and transformations of corresponding photo scenes by using 3D geometrical calculations. The Bundle Adjustment (BA) method is well known to improve the accuracy of the camera trajectories in the calculations. The refined camera positions can then be used to calculate a sparse 3D point-cloud of the target objects. Rather than using the ordinary Bundler open-source software [43], the multi-core bundle adjustment [56] within the VisualSFM open-source software [57] can minimise the computing time for the point-cloud data processing by performing both the CPU and GPU cores. It is also possible to gain more density of the point-cloud data by employing the Centre for Machine Perception-Multi-view Reconstruction (CMP-MVS) open-source software developed by Jancosek and Pajdla [25].

3.4. Fusion of top-view LiDAR and ground-view SfM data

Recent research has focused on the integration of data and models for more effective urban flood modelling that promise improved performance relative to accuracy [38,46]. Many studies have focused on enhancing the data quality [1–3,51]. Some research has implemented the single-view approach to obtain the data from almost the same source with different viewpoints for urban flood simulations [14,36]. However, it is still not clear whether the data fusion from both different sources and different viewpoints more effective.

In the previous steps, the single-view point-cloud data have been observed and processed, e.g., the top-view LiDAR data. At this step of process, each of the high-resolution point-cloud data may contain a large number of noises, which can be identified and cleaned by applying some of the filtering algorithms. Then, the single-view point-cloud data are ready to create a DTM directly, or it can be fused with other data sources by using multi-views approach for the next steps. To fuse the data, at least the two different data sources and/or different viewpoints are basically needed. The point-cloud data should be prepared in almost the same resolution, e.g., at same sub-metre resolutions for the high-resolution data. After that, the georeferencing points are carried on to rectify the entire point-cloud data into the correct global positioning system. The rectified point-cloud data are now ready to merge. As a result of that, million or trillion points are combined in the same single space. To create the DTM outputs in proper resolutions, thinning of the large point-cloud data should be performed beforehand. Finally, the vector point-cloud data are interpolated to the raster formats in the DTM creation step. The illustration of multi-view data fusion and DTMs creation steps is shown in Fig. 3.

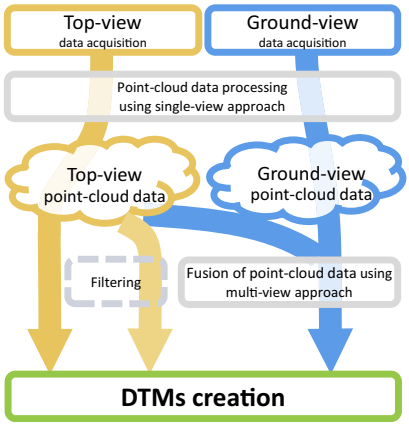

Fig. 3. Ways to create DTMs for coupled 1D–2D urban flood modelling.

4. Case study of Kuala Lumpur

4.1. Site conditions and event description

Kuala Lumpur, the capital city of Malaysia, is a densely populated urban area with an estimated population of over 3.6 million and is growing at almost 5% a year. The city is still experiencing considerable flooding from both rivers (the Klang River and the Gombak River) and from excess rainfall, which often cannot be contained by the local drainage system. Although major flood mitigation works have been implemented within the city, it continues to suffer from floods and flood-related damages. There are still major disruptions due to flooding.

A small area of Kuala Lumpur was chosen as a study case for exploring the effect of different ways of Digital Terrain Modelling. Some measurement data were available for a major flood event and a 1D numerical flood model had already been developed by DHI Water and Environment [11]. The complex urban area covered about 0.4 km^2 (for location see Fig. 4a, for area map see Fig. 4c) and was located at the confluence of the Klang River flowing from the

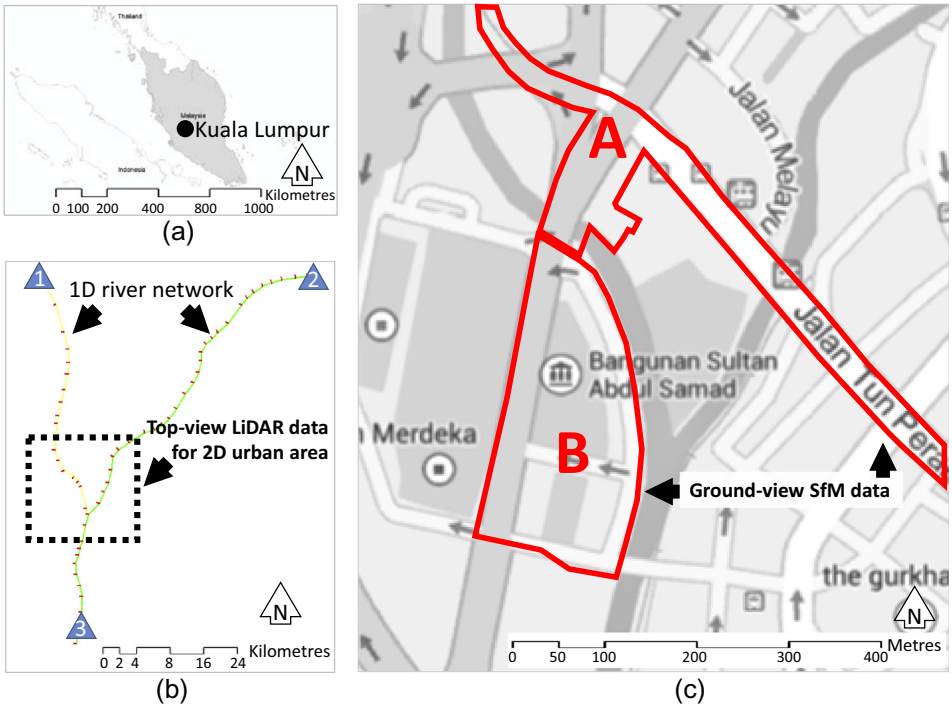

Fig. 4. (a) The city of Kuala Lumpur (Malaysia); (b) the coupled 1D–2D model schematization (1D river network and 2D urban area); (c) the two areas (marked "A" and "B") that were explored by the ground-view Structure from Motion technique (background from GoogleMap®).

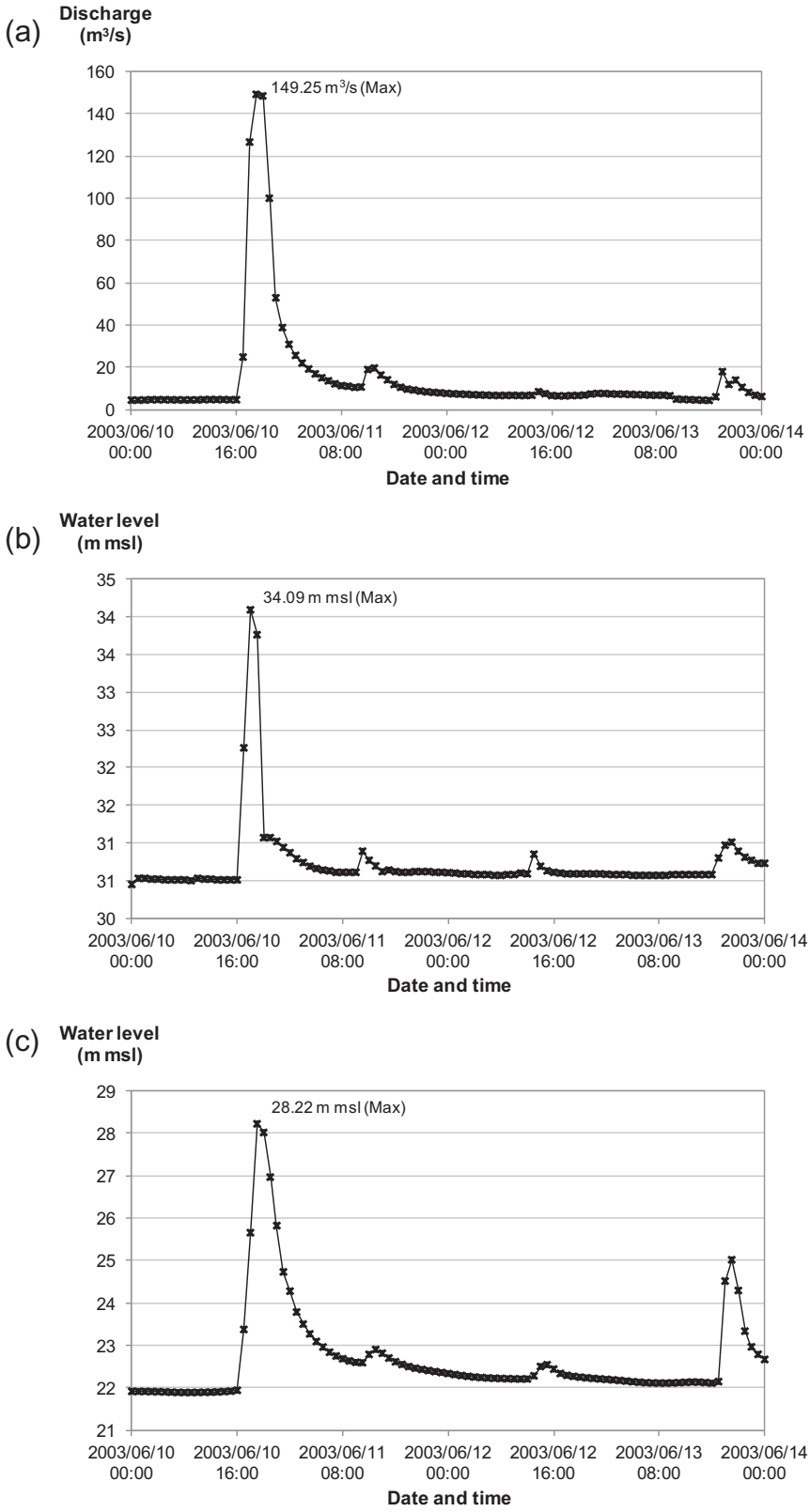

Fig. 5. Time-series data: (a) discharge at Jalan Tun Razak and (b) water level at Tun Razak Bonos; (c) water levels at Jambatan Sulaiman.

Northeast, and the Gombak River flowing from the Northwest. A coupled 1D–2D model of Kuala Lumpur had been further developed to investigate the propagation of excess floodwater from the two main rivers (the Klang and Gombak Rivers) into the 2D urban area (Fig. 4b), using the DHI MikeFlood® software. The flood event of 10 June 2003 was used as the case study. A Manning

friction coefficient n of 0.020 was applied uniformly to the constructed 1D channels, following the criteria defined by Chow [8]. A Manning coefficient n of 0.033 was used for the 2D urban surface area, applied identically to each of the three DTMs following an earlier study by Abdullah et al. [3]. Six measurement locations

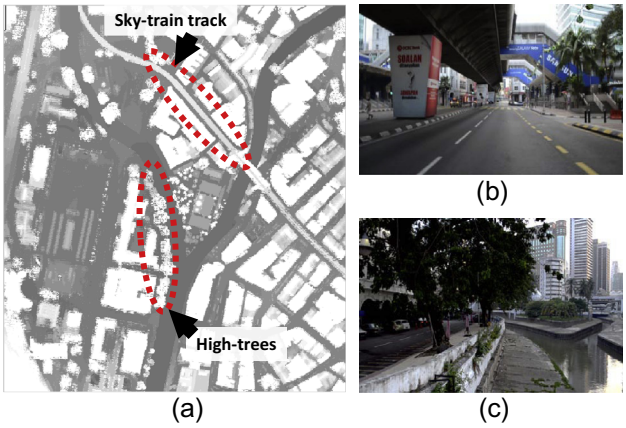

Fig. 6. (a) A standard top-view LiDAR-DTM; (b) the sky-train tracks and kerbs underneath; (c) the high trees and kerbs underneath.

Fig. 7. A filtered top-view LiDAR-DTM.

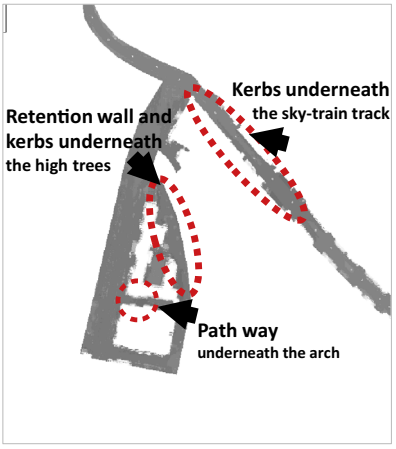

Fig. 8. Areas of ground-view SfM exploration.

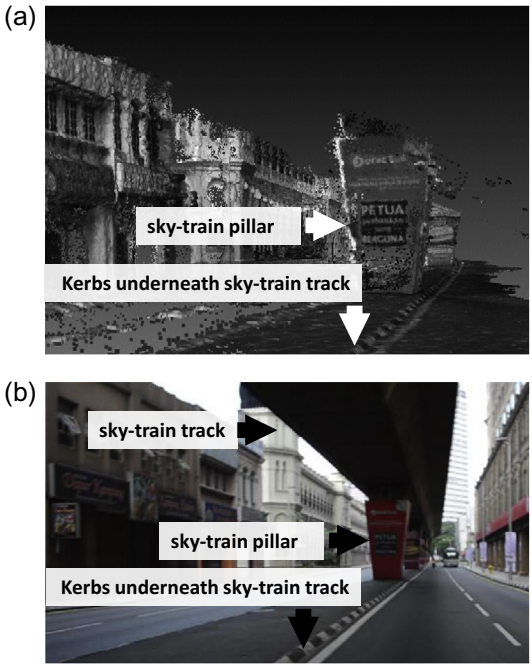

Fig. 9. (a) Ground-view SfM point-cloud image showing the sky-train track and kerbs underneath; (b) photo of actual sky-train track and kerbs.

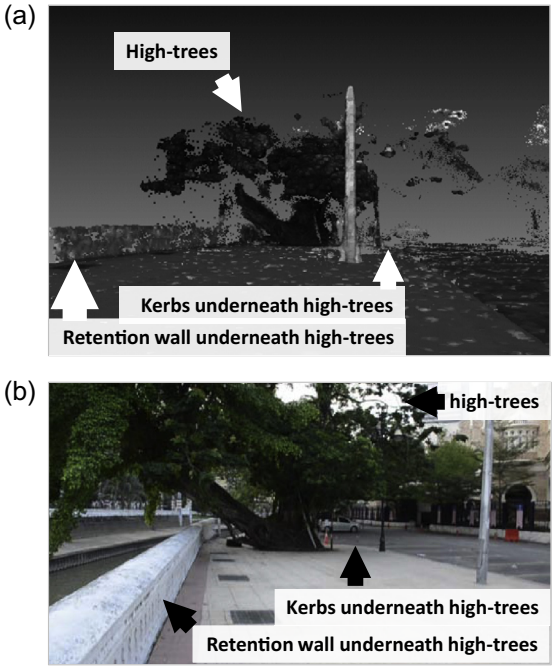

Fig. 10. (a) Ground-view SfM point-cloud image showing high trees and kerbs underneath; (b) photo of actual high trees and kerbs.

observed by the Department of Irrigation and Drainage (DID) were available to evaluate the flood simulation models.

4.2. Constructing three Digital Terrain Models

Three different types of Digital Terrain Models (DTMs) were constructed. The top-view LiDAR data provided by DID were used

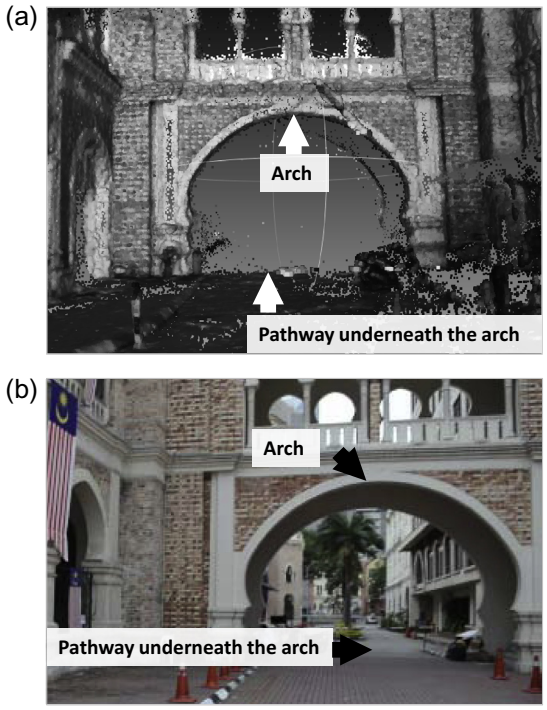

Fig. 11. (a) Ground-view SfM point-cloud data showing the arch and its pathway underneath; (b) photo of actual arch and pathway.

to create (i) a standard LiDAR-DTM and (ii) a Filtered LiDAR-DTM, as described hereafter in Sections 4.2.1 and 4.2.2 in more detail. In addition to these two DTMs, having collected ground-view SfM data for the two areas marked "A" and "B" in Fig. 4c, a novel 'Multidimensional Fusion of Views' approach was employed to construct (iii) a so-called multi-view Digital Terrain Model (MFV-DTM) by blending top-view LiDAR data and ground-view SfM data, as elaborated in Section 4.2.3.

4.2.1. Standard top-view LiDAR-DTM

An Airborne Laser Scanner (ALS) system utilising the LMS-Q560 LiDAR system with 75 kHz of effective signal and 60° field of view (FoV), was set and mounted on a Bell-206b Jet Ranger helicopter. The platform flew at an altitude of ~700 m with a ground speed of ~51.4 m/s to maintain 40% side lap at each flying path. An inertial measurement unit (IMU) was used and a global positioning system (GPS) provided an absolute accuracy of ±0.05 m in the horizontal direction and approximately twice as much in the vertical direction. The LiDAR data were collected with an average single run density of ~2.4 points per meter or a diameter of ~42 cm between each elevation point. Therefore, urban features smaller than this diameter could not be captured into this dataset.

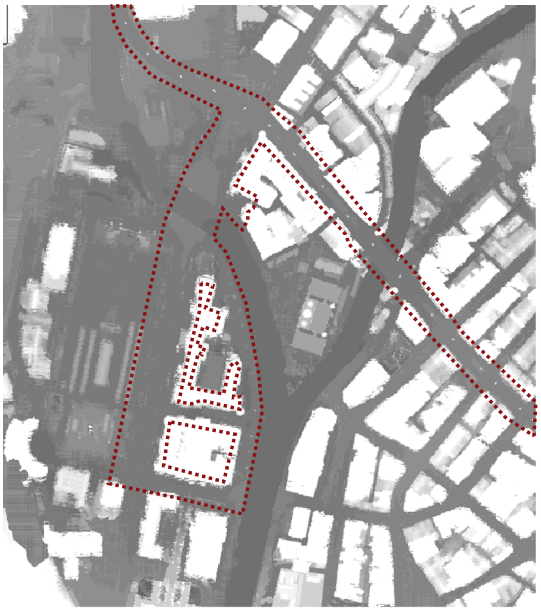

Fig. 13. Fusion of top-view LiDAR and ground-view SfM point-cloud data; the dotted line refers to the ground-view SfM data boundary.

By using a traditional single view approach, LiDAR point-cloud data needed to be processed and evaluated to detect specific urban features; sky-train track (see Fig. 6b); high trees (see Fig. 6c); other river crossing structures, that could mistakenly be perceived as obstructions to the floodwaters. These features were then removed from the DTM. The neighbouring elevations were then interpolated to fill in the actual river profile. Isolated points that were less than 10 neighbouring points within 0.5 m horizontal distance, were thinned and simplified to create the top-view LiDAR terrain map by using ArcGIS®. Finally, the point-cloud of the top-view LiDAR data was converted to obtain a standard LiDAR-DTM with upscaling to 1 m gridded resolution using MikeZero® (see Fig. 6a).

4.2.2. Filtered LiDAR-DTM

Following on from the previous step, a filtered top-view LiDAR point-cloud was constructed by removing high trees, elevated

Fig. 12. Example of a point-cloud data fusion obtained by blending the top-view LiDAR data with the ground-view SfM data.

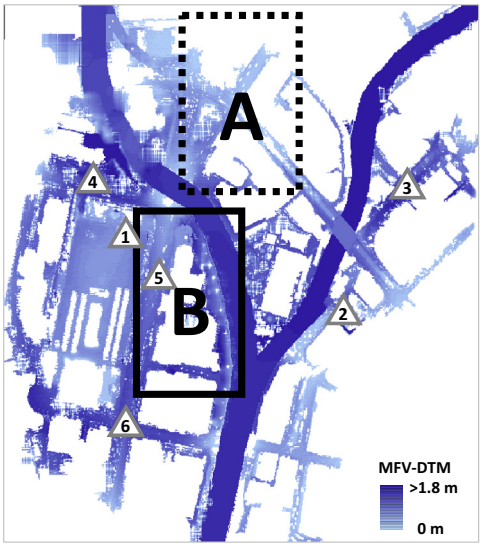

Fig. 14. Maximum flood depths using MFV-DTM as input; locations 1–6 indicate measurement locations of DID; the area marked by dotted line "A" refers to Fig. 15, the area marked by a solid line "B" refers to Fig. 16.

roads, and sky-train tracks following a previous study by Abdullah et al. [3]. The remaining neighbouring elevations were then interpolated again in order to replace the high urban features in ArcGIS®. The filtered point-cloud of the top-view LiDAR data was converted into a 1 m grid resolution to obtain the (ii) Filtered LiDAR-DTM in MikeZero® (see Fig. 7).

4.2.3. Ground-view SfM observations

A Nikon D5100 digital single-lens reflex (DSLR) camera was used as a video camcorder to record high definition videos of 1920 × 1080 pixels at 30 frames per second. More than 12 video scenes were recorded from a ground view along the streets of Jalan Tun Perak Road, and of the Bangunan Sultan Abdul Samad Building known as the high court of Kuala Lumpur City (see the locations marked "A" and "B" in Fig. 4c, resp.). An automated image separation process was used to slice the video scenes into a series of overlapping photos of the same resolution, using Python scripts. Even though the Vibration-Reduction (VR) technology of the Nikkor 18–55 mm lens was set to stabilize the video scenes, still some blurry scenes were recorded due to camera motion or object movement. A subsequent removal of blurred photos was undertaken manually. A laptop, running 64-bit Microsoft Windows 7 equipped with 8 cores Intel® i7 CPU at 2.20 GHz, 16 GB of RAM, and 2 GB Video RAM embedded in NVIDIA® GeForce™ GTX580M graphics cards was used for point-cloud data processing. Twenty distinct ground control points (GCPs) in the LiDAR dataset were used to reference the coordinate positions of the SfM point-cloud data. The absolute error in producing the ground-view SfM dataset (see Fig. 8) was found to be in the order of ~18 cm (RMSE in the GCP data). The ground-view SfM point cloud data compared with the actual situation are presented below for the sky-train track with the kerbs underneath (Fig. 9); high trees (Fig. 10); arch building and underneath pathway (Fig. 11).

Table 2
The computed inundation areas of 1D–2D simulations using three different DTMs as input.

	Inundation extent (m^2)
1D–2D model using LiDAR-DTM	128,870
1D–2D model using F.LiDAR-DTM	151,699
1D–2D model using MFV-DTM	156,824

4.2.4. Multidimensional Fusion of Views – the MFV-DTM

As described above, the single-view approach was applied to create both the top-view LiDAR/F.LiDAR dataset and the ground-view SfM dataset, focusing on the sub-meter spatial resolution. In this section, a novel approach based on Multidimensional Fusion of Views is introduced by combining 3D point-cloud data obtained from different data sources and different viewpoints.

First, the top-view LiDAR data (the black dotted box in Fig. 4b) and ground-view SfM data (areas "A" and "B" in Fig. 4c) were manually combined to create a Multidimensional Fusion of Views (MFV) point cloud data by using MeshLab® open source software. The example of MFV point-cloud data demonstrates the data blending from different sources and different viewpoints (see Fig. 12). Therefore, it can also have benefits from both a large coverage area of the top-view LiDAR data (~42 cm resolution) and a great level of detail of the ground-view SfM data (~18 cm resolution).

Then the fusion of the top-view LiDAR and ground-view SfM point-cloud data was simplified in ArcGIS® by thinning the isolated points which were less than 10 neighbouring points within a 0.5 m horizontal distance. The resulting fusion point-cloud data (see Fig. 13) were used to create the third DTM based on (iii) Multidimensional Fusion of Views – Digital Terrain Model (MFV-DTM), at 1 m grid resolution using MikeZero®.

5. Results

The 2003 flood event that occurred on June 10th had been observed by the Drainage and Irrigation Department (DID). At the Gombak River, the discharges at Jalan Tun Razak station (marked "1" in Fig. 4b) were over 149 m^3/s (see Fig. 5a). At the

Table 1
Comparison of numerical simulations versus measured floodwater depths at six locations for three different input DTMs; (%Diff. = |Measured − Simulated|/Measured * 100).

	Locations					
	Dataran Merdeka (1)		Leboh Ampang (2)		Jalan Meleka (3)	
	Flood depth (m)	% Diff.	Flood depth (m)	% Diff.	Flood depth (m)	% Diff.
Measurement	0.50		1.20		1.30	
1D–2D model using LiDAR-DTM	068.	36.0	1.39	15.8	1.49	14.6
1D–2D model using F.LiDAR-DTM	0.46	8.0	1.29	7.5	1.43	10.0
1D–2D model using MFV-DTM	0.47	6.0	1.28	6.7	1.40	7.7
	Jalan Parlimen (4)		Jalan Raja (5)		Leboh Pasar (6)	
	Flood depth (m)	% Diff.	Flood depth (m)	% Diff.	Flood depth (m)	% Diff.
Measurement	0.50		1.00		0.65	
1D–2D model using LiDAR-DTM	0.79	58.0	1.22	22.0	0.85	30.8
1D–2D model using F.LiDAR-DTM	0.46	8.0	1.08	8.0	0.72	10.8
1D–2D model using MFV-DTM	0.47	6.0	1.04	4.0	0.68	4.6

Klang River, the water levels at Tun Razak Bonos station (marked "2" in Fig. 4b) were over 34 m msl (see Fig. 5b), and the water levels at Jambatan Sulaiman station (marked "3" in Fig. 4b) were above 28 m msl (see Fig. 5c). Further to that, the water levels in rivers started to spill over the banks onto the Kuala Lumpur City. The flood simulation results were then evaluated of six measurement locations (marked "1" to "6" in Fig. 14).

From the results given in Table 1 we can observe that the largest difference (58%) in floodwater depths occurred at Jalan Parlimen (location "4" in Fig. 14). When applying a standard LiDAR-DTM as terrain input, the maximum depth in the simulation differs from the measurements by about +0.29 m. Conversely, when applying a F.LiDAR-DTM and MFV-DTM as input, these values are seen to reduce considerably down to 8.0% and 6.0%, resp. When applying the MFV-DTM, the simulation results differ from the measurements by only ±0.04 m for all six-measurement locations. The numerical simulation results also show that when there are fewer obstructions in the urban DTMs, the areas of flood propagation become larger (see Table 2).

Fig. 14 shows that the maximum flood depth is best simulated when using the new MFV-DTM as terrain input. In sub-regions "A" and "B" the detailed results of the time evolution of floodwater depths and flow velocities as presented in Figs. 15 and 16 shows that the floodwaters primarily propagate along the riverbanks, roads, pathways, and along other lowland areas. In sub-region "A", the flow is from the South to North. Floodwaters start to overflow from the Gombak River into the city at time step $t = 480$ (see Fig. 15a-1, b-1, and c-1). In sub-region "B" the floodwaters start to overflow from the Gombak River to the riverbank at the same time step $t = 480$ s (see Fig. 16a-1, b-1, and c-1).

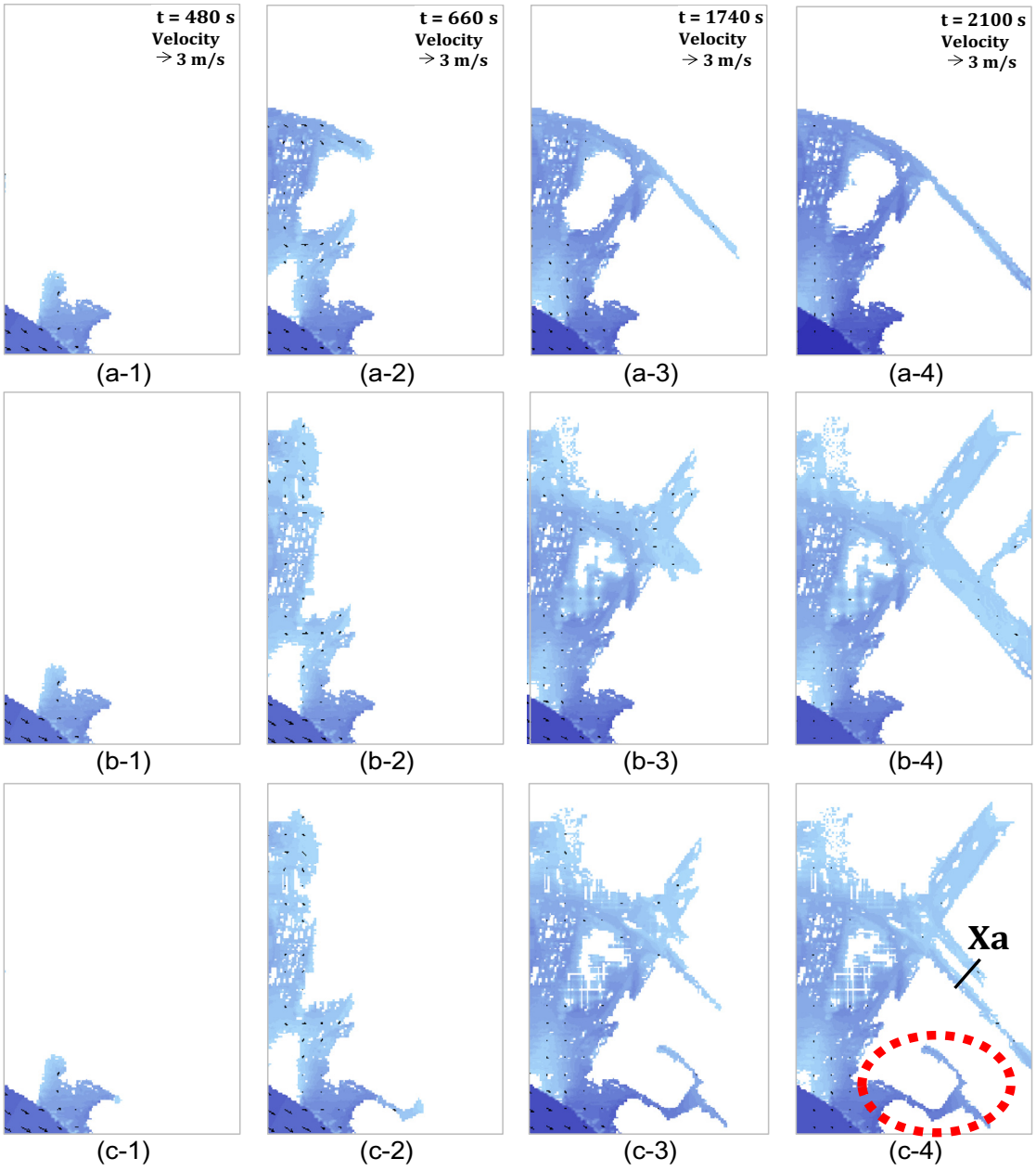

Fig. 15. Flood simulation results (floodwater depths and flow velocities) in sub-region "A" (Fig. 14) at time steps $t = 480$, 660, 1740, and 2100 s using LiDAR-DTM (a-1 to 4); F.LiDAR-DTM (b-1 to 4); MFV-DTM (c-1 to 4). The cross section "Xa" in (c-4) runs SW–NE and is referred to in detail in Fig. 17; the circular area in (c-4) marked with the dotted red line is elaborated in the text. (For interpretation of the references to color in this figure legend, the reader is referred to the web version of this article.)

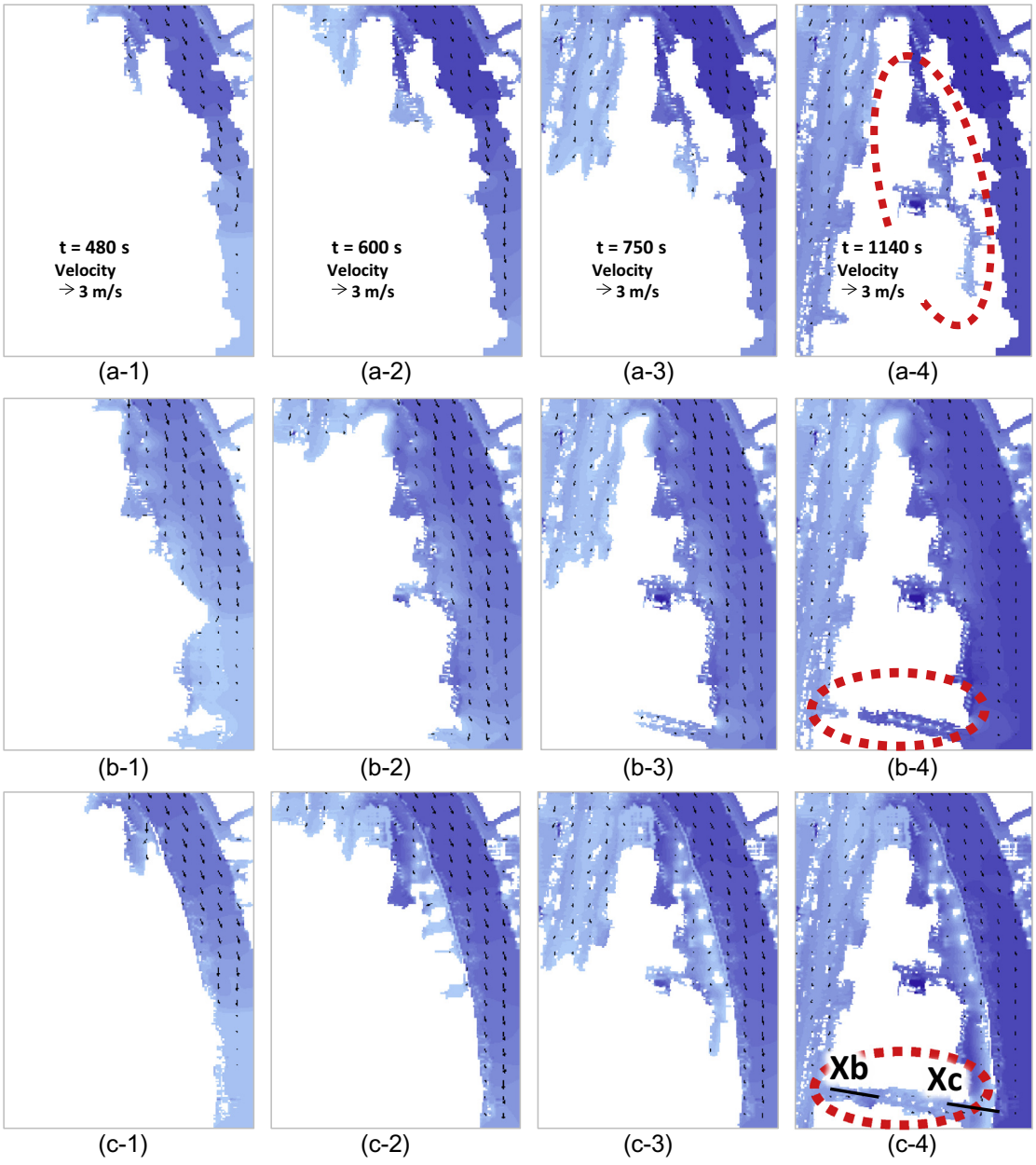

Fig. 16. Flood simulation results (floodwater depths and flow velocities) in sub-region "B" (Fig. 14) at time steps t = 480, 600, 750, and 1140 s using LiDAR-DTM (a-1 to 4); F.LiDAR-DTM (b-1 to 4); MFV-DTM (c-1 to 4). Cross sections "Xb" and "Xc" in (c-4) run W–E and are elaborated in Figs. 18 and 19, resp. The dotted areas in a-4, b-4, and c-4 are elaborated in the text.

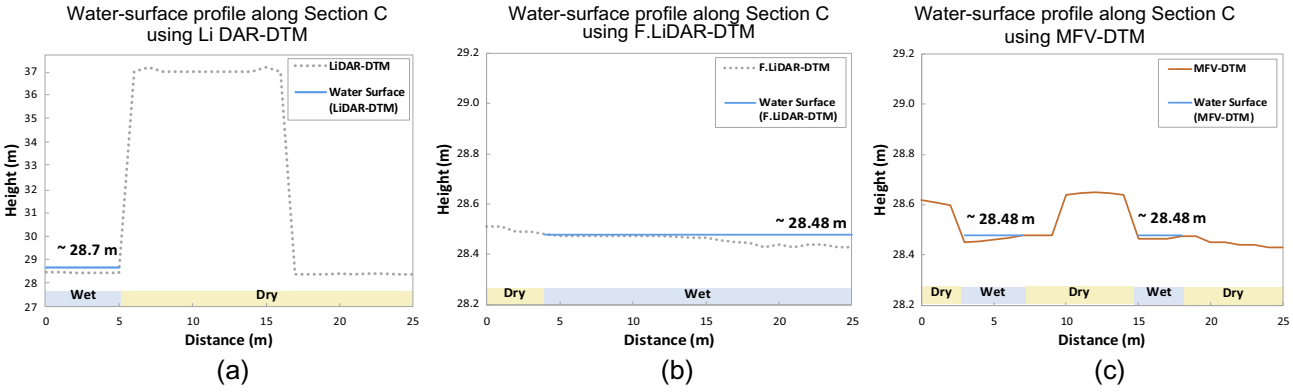

Fig. 17. Simulated water surface and elevation profiles for the three DTM inputs at cross section "Xa" in Fig. 15c-4.

5.1. Flood simulation results using a standard LiDAR-DTM

When applying a standard LiDAR-DTM as input data, the flood simulation results in sub-region "A" show that the higher flood depths accumulate in the middle part at time step $t = 600$ s and the flows are seemingly blocked by the sky train track, diverting the flows towards the S–E direction (Fig. 15a-1 to a-4). In sub-region "B", the floodwaters flow in the N–S direction (Fig. 16a-1 to a-4). The flood simulation results show that floodwaters accumulate along the riverbank in the Eastern part, and that floodwaters are confined between high trees and buildings (see the circular area marked with a dotted line in Fig. 16a-4).

5.2. Flood simulation results using a Filtered LiDAR-DTM

When applying a Filtered LiDAR-DTM (F.LiDAR-DTM) as input data, it is observed that the floodwaters in sub-region "A" can freely flow towards the Northern part of the domain without being blocked by the sky-train track (Fig. 15b-1 to b-4). In sub-region "B", the floodwaters flow in the N–S direction (Fig. 16b-1 to b-4). Floodwaters start to overflow directly from the Gombak River in the E-W part of the domain. The floodwaters flow over the riverbank towards the pathways before they are seemingly blocked by the arch of the Bangunan Sultan Abdul Samad Building at $t = 750$ s. It appears as if the floodwaters coming from the East cannot reach the floodwater from the West because of the arch (the area marked by a dotted line in Fig. 16b-4).

5.3. Flood simulation results using a Multidimensional Fusion of Views (MFV-DTM)

Although applying either a F.LiDAR-DTM or a Multidimensional Fusion of Views (MFV-DTM) shows that floodwaters can now freely flow into the Northern part of the domain in sub-region A, the results illustrate that some inundated parts can only be exposed when employing the MFV-DTM (see the dotted circle in Fig. 15c-4) which is capable of capturing small urban features (e.g., pathways and kerbs). In sub-region "B", floodwaters do not come directly from the river in the East, but first start to overflow from the Gombak River in the North before flowing into the urban area in the South. Small urban features such as retention walls and kerbs will divert some floodwaters flowing along the riverbank and alleyways (see Fig. 16c-2 to c-4). In addition, floodwaters can connect with the other side at $t = 1140$ s (see the dotted area in Fig. 16c-4).

When considering the longitudinal profile of cross section "Xa" (Fig. 15c-4), it can be observed that for LiDAR-DTM as input, the floodwaters are confined to the zone on the left side (Fig. 17a), while applying F.LiDAR-DTM shows that the floodwaters inundate most of the cross section (Fig. 17b). On the other hand, using MFV-DTM, floodwaters are diverted and separated by small kerbs (see Fig. 17c).

The second longitudinal cross section (Xb in Fig. 16c-4) shows floodwater depth patterns in more detail When applying LiDAR-DTM as input, floodwaters are confined to the Gombak River on the left side (see Fig. 18a). Applying F.LiDAR-DTM shows that floodwaters are seemingly blocked by the arch of the Bangunan

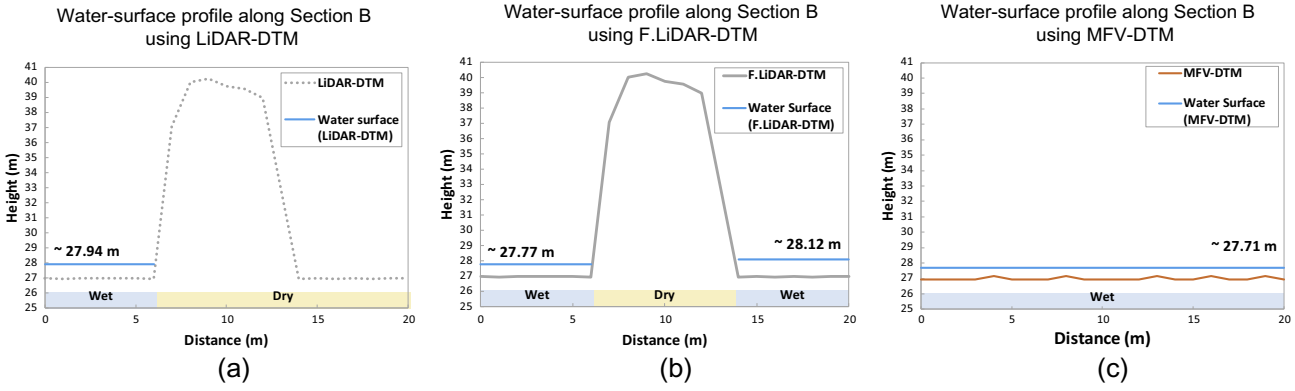

Fig. 18. Simulated water surface and elevation profiles for: (a) LiDAR-DTM, (b) F.LiDAR-DTM, and (c) MFV-DTM, at time steps $t = 1140$ s, at cross section "Xb" in Fig. 16c-4.

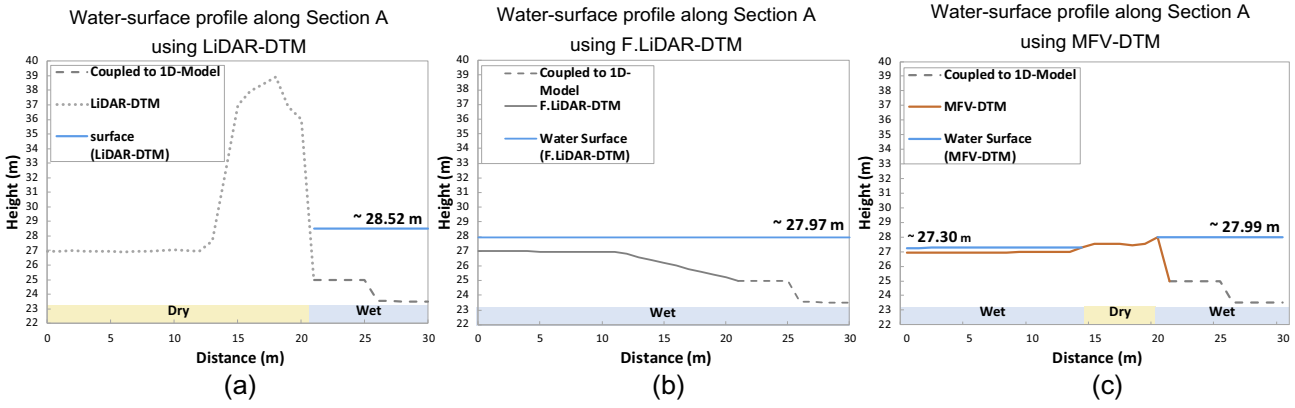

Fig. 19. Simulated water surface and elevation profiles for: (a) LiDAR-DTM, (b) F.LiDAR-DTM, and (c) MFV-DTM, at time steps $t = 1140$ s, at cross section "Xc" in Fig. 16c-4.

Sultan Abdul Samad Building (see Fig. 18b), showing the separate wet zone on the left side (the riverside) and another on the right side (the roadside). On the other hand, using MFV-DTM, floodwaters can flow freely from the river side into the roadside, or the other way around (see Fig. 18c).

The third longitudinal profile of cross section "Xc" in Fig. 16c-4 also shows that when applying LiDAR-DTM as input, floodwaters are confined to the wet zone of the Gombak River on the right side (see Fig. 19a). Applying F.LiDAR-DTM shows that floodwaters flow freely from the river on the left side to the riverbank on the right side (see Fig. 19b). Using MFV-DTM, floodwaters are seen to be diverted by small retention walls and kerbs along the riverbank, separating the floodwaters from the left (riverbank) side to the right (river) side (see Fig. 19c).

6. Discussion

The flood simulation results presented here show that incorporation of urban features (sky-train tracks, elevated roads, high trees) in a numerical model is an important aspect as such features can cause and can play a significant role in diverting the shallow flows that are generated in urban environments.

When using (i) a standard LiDAR-DTM input, some high features (i.e., sky-train tracks) are seen to behave as dikes (see the cross section "Xa" in Fig. 15c-4 and details in Fig. 17). The floodwaters seem to propagate only in the Southern direction and no floodwater appears in the Northern part of the domain (see the sub-region "A" and details in Fig. 15a-2 to a-4). In sub-region "B", the high trees (the circular area marked by a dotted line in Fig. 16a-4) look like an island (see the cross section "Xc" in Fig. 16c-4 and details in Fig. 19), seemingly obstructing floodwater flows from the Gombak River in the East.

When applying (ii) a F.LiDAR-DTM approach (see Fig. 7), the filtered data replace the high features (sky train tracks and high trees) with ground-flatted elevations. However, it is not possible to correctly create or reconstruct the small urban features hidden underneath the high features. Nevertheless, such (hidden) small urban features can have a considerable effect on floodwater dynamics and predictions [34–36]. By applying the F.LiDAR-DTM as input, flood simulation results have misrepresented floodwater propagations (see the area marked by the dotted line in Fig. 15b-4 and c-4) and mismatch floodwater depths (see the cross section "Xa" in Fig. 15c-4 and details in Fig. 17).

When including SfM data it is possible to take into account small urban features by using (iii) a Multidimensional Fusion of Views (MFV-DTM) approach. This new approach can represent even small details of urban features that can still play a significant role in diverting shallow floodwaters. As a result, floodwater propagation can be predicted much better. It is observed that small kerbs (sideways and middle parts of Jalan Tun Perak Road) play a significant role in diverting and confining floodwaters flowing along the road. In sub-region "B" (see Fig. 14), floodwaters can now flow freely through alleyways without any obstruction by arches. The results also show that small urban features located along river banks (i.e., retention walls and kerbs) can play an important role in diverting floodwater patterns (see the cross sections "Xc" in Fig. 16c-4 and details in Fig. 19). It can be noted that applying the new MFV-DTM approach can represent more details of riverbank structures as well as hidden small urban features such as pathways, retention walls, and sidewalk kerbs.

7. Conclusions

The results obtained from the present work show that the proposed technique based on fusion of LiDAR data and Structure from Motion observations can be very beneficial for flood modelling applications. In the cases study work presented here, a 1D-2D numerical modelling approach was used to simulate the extreme urban flooding event that occurred on 10th June 2003 in Kula Lumpur (Malaysia). The three different digital terrain maps (DTMs) were derived from top-view LiDAR data and ground-view Structure from Motion (SfM) observations.

From the analysis, it was found that when employing a standard LiDAR-DTM the flow patterns and water depths may not be correctly represented in the digital terrain map since overarching structures such as a sky train or elevated roads are usually perceived as obstructions for floodwater propagation. Some of these obstructing features could be removed by applying some of the filtering algorithms in the LiDAR-DTM data set. However, in the filtered digital terrain map the obstructing features can only be replaced with the surrounding ground-flattened elevations that do not contain particular urban features hidden underneath. Present work has shown that a ground-based SfM technique can be effective in detecting small urban features (e.g., arches, retention walls, alleyways, and kerbs). Correspondingly, the numerical flood simulation results were found to be not only in a good agreement with floodwater depth observations, but also to better represent the floodwater dynamics in a more detail. Such detailed models are of increasing concern to insurance sectors to evaluate the primary drivers of the flood damages and losses [13]. It should also help to assess road network drainage capability to both the public sector for critical infrastructure planning and to the private sector for business interruption loss estimation [36].

Overall, it can be concluded that the new multi-view approach of combining the top-view LiDAR data with the ground-view SfM observations is capable of creating a more accurate digital terrain map, which can be then used as an input for numerical urban flood model simulations and produce a more realistic representation of floodwater dynamics and inundation depths. Future work in fusing remotely sensed data from SfM-based surveys to create both the top-view and side-view images has already been undertaken, thus enabling a rapid setup of numerical flood models over larger domains.

Acknowledgments

The work presented in this paper was carried out as part of a PhD research project funded by OCSC and HAII, the Ministry of Science and Technology (Thailand). The authors would like to express their gratitude to DID (Malaysia) for providing the LiDAR and hydrological data for the case study. The support from N.A. Aziz and A. Pramuanjaroenkij for their advice and assistance with data collection and processing is greatly appreciated.

References

[1] Abdullah AF, Rahman A, Vojinovic Z. LiDAR filtering algorithms for urban flood application: review on current algorithms and filters test. In: 8th International conference on urban drainage modelling. Tokyo, Japan; 2009. http://dx.doi.org/10.2166/hydro.2011.009.

[2] Abdullah AF, Vojinović Z, Price RK, Aziz NAA. Improved methodology for processing raw LiDAR data to support urban flood modelling – accounting for elevated roads and bridges. J Hydroinform 2012;14(2):253–69. http://dx.doi.org/10.2166/hydro.2011.009.

[3] Abdullah AF, Vojinović Z, Price RK, Aziz NAA. A methodology for processing raw LiDAR data to support urban flood modelling framework. J Hydroinform 2012;14(1):75–92. http://dx.doi.org/10.2166/hydro.2011.089.

[4] Boonya-aroonnet S. Applications of the innovative modelling of urban surface flooding in the UK case studies. In: 11th International conference on urban drainage, Edinburgh, UK; 2010.

[5] Casas A, Riaño D, Greenberg J, Ustin S. Assessing levee stability with geometric parameters derived from airborne LiDAR. Remote Sens Environ 2012;117:281–8. http://dx.doi.org/10.1016/j.rse.2011.10.003.

[6] Chen AS, Hsu MH, Teng WH, Huang CJ, Yeh SH, Lien WY. Establishing the database of inundation potential in Taiwan. Nat Hazards 2006;37:107–32. http://dx.doi.org/10.1007/s11069-005-4659-7.

[7] Chen AS, Evans B, Djordjević S, Savić DA. Multi-layered coarse grid modelling in 2D urban flood simulations. J Hydrol 2012;470–471:1–11. http://dx.doi.org/10.1016/j.jhydrol.2012.06.022.

[8] Chow VT. Open-channel hydraulics. New York: McGraw-Hill; 1959.

[9] Clarke TA, Fryer JG. The development of camera calibration methods and models. Photogramm Rec 1998;16(91):51–66. http://dx.doi.org/10.1111/0031-868X.00113.

[10] Cunge JA, Holly FM, Verwey A. Practical aspects of computational river hydraulics: monographs and surveys in water resources engineering. London: Pitman Publishing Ltd; 1980.

[11] DHI Water & Environment. Klang River-basin environment improvement and flood mitigation project (Stormwater Management and Road Tunnel – SMART). Final report. Department of Irrigation and Drainage, Malaysia; 2004.

[12] Djordjević S, Prodanović D, Walters G. Simulation of transcritical flow in pipe/channel networks. J Hydraul Eng 2004;130:1167–78. http://dx.doi.org/10.1061/(ASCE)0733-9429(2004)130:12(1167).

[13] Evans EP, Simm JD, Thorne CR, Arnell NW, Hess TM, Lane SN. The Pitt review: an update of the foresight future flooding 2004 qualitative risk analysis. London: Cabinet Office; 2008.

[14] Fewtrell TJ, Duncan A, Sampson CC, Neal JC, Bates PD. Benchmarking urban flood models of varying complexity and scale using high resolution terrestrial LiDAR data. Phys Chem Earth Pt A/B/C 2011;36(7–8):281–91. http://dx.doi.org/10.1016/j.pce.2010.12.011.

[15] Goesele M, Snavely N, Curless B, Hoppe H, Seitz SM. Multi-view stereo for community photo collections. In: IEEE 11th ICCV. Rio de Janeiro, Brazil; 2007. http://dx.doi.org/10.1109/ICCV.2007.4408933.

[16] Hai PT, Magome J, Yorozuya A, Inomata H, Fukami K, Takeuchi K. Large-scale flooding analysis in the suburbs of Tokyo Metropolis caused by levee breach of the Tone River using a 2D hydrodynamic model. Water Sci Technol 2010;62:1859–64. http://dx.doi.org/10.2166/wst.2010.381.

[17] Haile AT, Rientjes TH. Effects of LiDAR DEM resolution in flood modelling: a model sensitivity study for the city of Tegucigalpa, Honduras. In: 36th ISPRS workshop 'laser scanning'. Enschede, The Netherlands; 2005.

[18] Hervouet J, Janin J. Finite element algorithms for modelling flood propagation. In: Proceedings, modelling of flood propagation over initially dry areas. Milan, Italy; 1994.

[19] Hervouet J, Van Haren L. Recent advances in numerical methods for fluid flow. In: Anderson MG, Walling DE, Paul DB, editors. Floodplain processes. Chichester: Wiley; 1996. p. 183–214.

[20] Hestholm S, Ruud B. 2D finite-difference elastic wave modelling including surface topography. Geophys Prospect 1994;42:371–90. http://dx.doi.org/10.1111/j.1365-2478.1994.tb00216.x.

[21] Horritt MS, Bates PD. Effects of spatial resolution on a raster based model of flood flow. J Hydrol 2001;253:239–49. http://dx.doi.org/10.1016/S0022-1694(01)00490-5.

[22] Hsu MH, Chen SH, Chang TJ. Inundation simulation for urban drainage basin with storm sewer system. J Hydrol 2000;234:21–37. http://dx.doi.org/10.1016/S0022-1694(00)00237-7.

[23] Hunter NM, Bates PD, Neelz S, Pender G, Villanueva I, Wright NG, Liang D, Falconer RA, Lin B, Waller S. Benchmarking 2D hydraulic models for urban flooding. P Ice-water Manage 2008;161:13–30. http://dx.doi.org/10.1680/wama.2008.161.1.13.

[24] Irschara A, Zach C, Klopschitz M, Bischof H. Large-scale, dense city reconstruction from user-contributed photos. Comput Vis Image Und 2012;116(1):2–15. http://dx.doi.org/10.1016/j.cviu.2011.07.010.

[25] Jancosek M, Pajdla T. Multi-view reconstruction preserving weakly-supported surfaces. In: IEEE conference on CVPR, CO, USA; 2011. http://dx.doi.org/10.1109/CVPR.2011.5995693.

[26] Lowe DG. Distinctive image features from scale-invariant keypoints. Int J Comput Vision 2004;60:91–110. http://dx.doi.org/10.1023/B:VISI.0000029664.99615.94.

[27] Luscombe BW, Hassan HM. Applying remote sensing technologies to natural disaster risk management: implications for developmental investments. Acta Astronaut 1993;29(10–11):871–6. http://dx.doi.org/10.1016/0094-5765(93)90169-W.

[28] Mark O, Weesakul S, Apirumanekul C, Boonya-aroonnet S, Djordjević S. Potential and limitations of 1D modelling of urban flooding. J Hydrol 2004;299:284–99. http://dx.doi.org/10.1016/j.jhydrol.2004.08.014.

[29] Marks K, Bates PD. Integration of high-resolution topographic data with floodplain flow models. Hydrol Process 2000;14:2109–22. http://dx.doi.org/10.1002/1099-1085(20000815/30)14:11/12<2109::AID-HYP58>3.0.CO;2-1.

[30] Mitasova H, Hardin E, Starek MJ, Harmon RS, Overton MF, Hengl T, Evans I, Wilson J, Gould M. Landscape dynamics from LiDAR data time series. In: Geomorphometry. CA, USA; 2011.

[31] Neal JC, Bates PD, Fewtrell TJ, Hunter NM, Wilson MD, Horritt MS. Distributed whole city water level measurements from the Carlisle 2005 urban flood event and comparison with hydraulic model simulations. J Hydrol 2009;368:42–55. http://dx.doi.org/10.1016/j.jhydrol.2009.01.026.

[32] Puente I, González-Jorge H, Martínez-Sánchez J, Arias P. Review of mobile mapping and surveying technologies. Measurement 2013;46:2127–45. http://dx.doi.org/10.1016/j.measurement.2013.03.006.

[33] Razafison U, Cordier S, Delestre O, Darboux F, Lucas C, James F. A shallow water model for the numerical simulation of overland flow on surfaces with ridges and furrows. Eur J Mech B-Fluids 2012;31:44–52. http://dx.doi.org/10.1016/j.euromechflu.2011.07.002.

[34] Remondino F, El-Hakim S. Image-based 3D modelling: a review. Photogramm Rec 2006;21(115):269–91. http://dx.doi.org/10.1111/j.1477-9730.2006.00383.x.

[35] Rychkov I, Brasington J, Vericat D. Computational and methodological aspects of terrestrial surface analysis based on point clouds. Comput Geosci 2012;42:64–70. http://dx.doi.org/10.1016/j.cageo.2012.02.011.

[36] Sampson CC, Fewtrell TJ, Duncan A, Shaad K, Horritt MS, Bates PD. Use of terrestrial laser scanning data to drive decimetric resolution urban inundation models. Adv Water Resour 2012;41:1–17. http://dx.doi.org/10.1016/j.advwatres.2012.02.010.

[37] Schelfault K, Pannemans B, Van Der Craasts I, Krywkow J, Mysiak J, Cools J. Bringing flood resilience into practice: the FREEMAN project. Environ Sci Policy 2014;14(7):825–33. http://dx.doi.org/10.1016/j.envsci.2011.02.009.

[38] Schubert JE, Sanders BF, Smith MJ, Wright NG. Unstructured mesh generation and landcover-based resistance for hydrodynamic modeling of urban flooding. Adv Water Resour 2008;31(12):1603–21. http://dx.doi.org/10.1016/j.advwatres.2008.07.012.

[39] Schubert JE, Sanders BF. Building treatments for urban flood inundation models and implications for predictive skill and modeling efficiency. Adv Water Resour 2012;41:49–64. http://dx.doi.org/10.1016/j.advwatres.2012.02.012.

[40] Smeeckaert J, Mallet C, David N, Chehata N, Ferraz A. Large-scale classification of water areas using airborne topographic LiDAR data. Remote Sens Environ 2013;138:134–48. http://dx.doi.org/10.1016/j.rse.2013.07.004.

[41] Smith DI. Actual and potential flood damage: a case study for urban Lismore, NSW, Australia. Appl Geogr 1981;1(1):31–9. http://dx.doi.org/10.1016/0143-6228(81)90004-7.

[42] Smith RAE, Bates PD, Hayes C. Evaluation of a coastal flood inundation model using hard and soft data. Environ Modell Softw 2012;30:35–46. http://dx.doi.org/10.1016/j.envsoft.2011.11.008.

[43] Snavely N, Seitz SM, Szeliski R. Photo tourism: exploring photo collections in 3D. In: Proceedings, ACM SIGGRAPH; 2006. http://dx.doi.org/10.1145/1179352.1141964.

[44] Snavely N, Simon I, Goesele M, Szeliski R, Seitz SM. Scene reconstruction and visualization from community photo collections. In: Proceedings of the IEEE; 2010. http://dx.doi.org/10.1109/JPROC.2010.2049330.

[45] Stelling G, Kernkamp H, Laguzzi M. Delft flooding system: a powerful tool for inundation assessment based upon a positive flow simulation. In: HIC. Copenhagen, Denmark; 1998.

[46] Tsubaki R, Fujita I. Unstructured grid generation using LiDAR data for urban flood inundation modelling. Hydrol Process 2010;24(11):1404–20. http://dx.doi.org/10.1002/hyp.7608.

[47] Tuite K, Snavely N, Hsiao D, Tabing N, Popovic Z. PhotoCity: training experts at large-scale image acquisition through a competitive game. In: Proceedings, CHI; 2011. http://dx.doi.org/10.1145/1978942.1979146.

[48] Vojinović Z, Tutulic D. On the use of 1D and coupled 1D–2D modelling approaches for assessment of flood damage in urban areas. Urban Water J 2009;6:183–99. http://dx.doi.org/10.1080/15730620802566877.

[49] Vojinović Z, Seyoum SD, Mwalwaka JM, Price RK. Effects of model schematisation, geometry and parameter values on urban flood modelling. Water Sci Technol 2011;63:462–7. http://dx.doi.org/10.2166/wst.2011.244.

[50] Vojinović Z, Abbott MB. Flood risk and social justice: from quantitative to qualitative flood risk assessment and mitigation. London: IWA Publishing; 2012.

[51] Vojinović Z, Seyoum S, Salum MH, Price RK, Abdullah AF, Abebe Y. Modelling floods in urban areas and representation of buildings with a method based on adjusted conveyance and storage characteristics. J Hydroinform 2013;15(4):1150–68. http://dx.doi.org/10.2166/hydro.2012.181.

[52] Wang CK, Philpot WD. Using airborne bathymetric LiDAR to detect bottom type variation in shallow waters. Remote Sens Environ 2007;106:123–35. http://dx.doi.org/10.1016/j.rse.2006.08.003.

[53] Wendel A, Maurer M, Graber G, Pock T, Bischof H. Dense reconstruction on-the-fly. In: 2012 IEEE conference on CVPR. RI, USA; 2012. http://dx.doi.org/10.1109/CVPR.2012.6247833.

[54] Westoby MJ, Brasington J, Glasser NF, Hambrey MJ, Reynolds JM. 'Structure-from-motion' photogrammetry: a low-cost, effective tool for geoscience applications. Geomorphology 2012;179:300–14. http://dx.doi.org/10.1016/j.geomorph.2012.08.021.

[55] Wu CC. SiftGPU: a GPU implementation of scale invaraint feature transform (SIFT), 2007. <http://cs.unc.edu/~ccwu/siftgpu> [accessed January 2014].

[56] Wu CC, Agarwal S, Curless B, Seitz SM. Multicore bundle adjustment. In: IEEE international conference on CVPR. CO, USA; 2011. http://dx.doi.org/10.1109/CVPR.2011.5995552.

[57] Wu CC. VisualSFM: a visual structure from motion system. <http://homes.cs.washington.edu/~ccwu/vsfm> [accessed January 2014].